



# Configuration and Force-field Aware Variable Impedance Control with Faster Re-learning

Shail Jadav<sup>1</sup> · Harish J. Palanthandlam-Madapusi<sup>1</sup>

Received: 27 March 2023 / Accepted: 17 November 2023 / Published online: 18 December 2023  
© Springer Nature B.V. 2023

## Abstract

Variable impedance control (VIC) is rapidly becoming an important ingredient for robotic manipulation in unstructured and uncertain environments. In such situations, it is often necessary to rapidly adapt to different impedance levels as per the task requirements, and to return to a low baseline impedance for safety requirements. Such a capability is crucial to stabilize interactions in divergent force fields, which commonly arise in a variety of contact and force production tasks and occasionally in non-contact tasks. Conventional methods, such as iterative learning control, often underperform in terms of stabilization and efficacy. While VIC algorithms perform better, typical challenges in such methods include unnecessarily high impedance adaptation in divergent fields, difficulty in distinguishing between error-independent and error-based divergent forces, and reliance on the Jacobian inverse which diminishes performance near singularities. In this paper, we introduce an innovative VIC algorithm that addresses typical VIC challenges. The proposed method employs a Cartesian-space field adaptation avoiding the need for inverting the Jacobian during adaptation, while at the same time providing a theoretical stabilization guarantee. Utilizing the Lyapunov function, the algorithm is shown to drive tracking errors to zero, even in the presence of divergent position and velocity-error fields and error-independent forces. Notably, the system exhibits human-like relearning at a faster pace when exposed to previously learned fields or perturbations, improving learning speeds by up to 47.97%. Performance validation was conducted through simulations on a two-link serial chain manipulator that mimics the human arm, as well as tests on a seven degrees-of-freedom KUKA robot, underscoring the algorithm's advantages in handling VIC challenges and uncertain conditions.

**Keywords** Adaptive · Impedance · Human-like · Robotics · Control

## 1 Introduction

Robots are being increasingly designed for interacting with unstructured and uncertain environments including with humans, and as a result, there is a pressing need for control algorithms that can operate reliably in variable and uncertain environments. One such approach is variable-impedance control (VIC). These controllers are designed to adjust the impedance of the robot's end-effector in a manner analogous to how humans adapt their impedance when manipulating objects and interacting with the environment. In unstructured

and uncertain environments, it is often necessary to rapidly adapt to different impedance levels as per the task requirements and to return to a low baseline impedance for safety requirements. Such a capability is crucial to stabilize interactions in divergent force fields, which commonly arise in a variety of contact and force production tasks and occasionally in non-contact tasks.

Humans demonstrate remarkable adaptability in their interactions with the environment. Mechanically, they exhibit an exceptional ability to modulate their impedance, especially stiffness, during these interactions [1, 2]. This adaptability is further enhanced by humans' capacity to learn and optimize appropriate stiffness behavior for specific tasks through repetitive practice [2, 3]. Moreover, humans can adapt and stabilize their interactions even in the face of unexpected and destabilizing force-fields [2]. Developing similar capabilities in robotic systems remains an open and active area of research [4, 5]. The development of VIC is fundamen-

✉ Shail Jadav  
shail.jadav@iitgn.ac.in

Harish J. Palanthandlam-Madapusi  
harish@iitgn.ac.in

<sup>1</sup> SysIDEA Robotics Lab, IIT Gandhinagar, Palaj, Gandhinagar 382355, Gujarat, India

tally inspired by the human ability to modulate impedance. According to [6], human learning mechanisms go beyond simple stabilization, encompassing a complex array of traits such as savings, retention, and generalization. Savings refers to the accelerated relearning speed humans exhibit when they re-encounter a previously experienced perturbation after a period of non-exposure [7]. Retention, on the other hand, involves the observation of a reduced error magnitude during the re-perturbation phase [8]. Furthermore, humans' capability for generalization, which means quickly learning tasks similar to those previously mastered, is noteworthy [9]. These human motor learning characteristics bear significant potential for robotic systems' development. Nonetheless, current VIC methods [10] do not adequately mirror these human traits.

VIC can be effectively deployed to achieve stable and accurate movement when robots are operating under the effect of a *divergent force-field* [4, 5]. A divergent force field is a field that applies forces that tend to pull the robot end-effector away from the equilibrium position or from the nominal trajectory. Further, as the end-effector moves away from the equilibrium, the magnitude of the destabilizing force increases thus making it harder to return to the equilibrium and thus causing a divergent effect. Such force fields arise in a wide variety of day-to-day tasks, primarily in contact tasks but sometimes also in non-contact tasks. Some simple examples of divergent effect in day-to-day tasks include when holding on to a slippery boiled egg or pressing down on a tool. It is possible to manage divergent force-fields in simpler environments through the use of high-impedance controllers or with VICs that adapt to high levels of impedance without emphasis on subsequent de-adaptation (that is, return back to a lower baseline impedance). However, when considering robots assisting humans in more dynamic settings like kitchens [11], operating robots in high impedance may be unsafe. Impedance levels that are higher than required could result in a shattered glass jar or bruised produce. Therefore, it's crucial to have controllers that can rapidly modify their impedance based on the specific task, prioritizing both efficiency, stability, and safety.

Current VIC controllers fall largely into two categories, nonlinear-adaptive-control-based methods, and data-driven-learning-based methods. In nonlinear control-based methodologies, adaptive controllers adapt manipulator parameters based on the tenets of Lyapunov-based stability [4, 5, 12]. These techniques are fundamental in tool manipulation and highlight the importance of interaction stability [13, 14]. Several works extensively explore stability issues arising from modeling uncertainties, varying impedance dynamics, and iterative learning paradigms [15–18]. However, the requirement for precise knowledge of robotic parameters challenges both passivity and Lyapunov-based theories [10]. Such constraints have spurred interest in data-driven approaches, such

as reinforcement learning (RL). RL applications in robot-environment interactions are evolving, predominantly using neural networks, Q-Learning, and VIC strategies [19–23]. The focus is increasingly on refining impedance control, from dual-stage mechanisms to methods that learn from expert demonstrations [24, 25]. Moreover, the importance of stability in RL is evident, with discussions emphasizing consistent and certified stability solutions [26]. However, RL-based VICs face limitations. Strict safety requirements may limit exploration and risk leading to suboptimal policies [10].

Modern VIC methods often continue impedance adaptation beyond achieving optimal stabilization. This is largely because many algorithms depend on tracking errors for adaptation. As a consequence, they might make unwarranted adaptation driven by minor errors due to disturbances or noise [4, 5, 10, 21]. While this approach enhances tracking accuracy, it raises energy consumption and might increase safety risks, particularly in human-robot interactions. Further, VIC can adjust impedance in either joint or operational (Cartesian) space. Joint-space adaptation mainly considers joint-space errors, resulting in sub-optimal impedance modifications. As the controller refines joint-space stiffness, the subsequent transfer to Cartesian space is inefficient because of the manipulator Jacobian [27]. With persistent Cartesian stiffness disturbances, the robot tends to learn diverse joint-space stiffness values, usually tuning to the most stable one. This becomes an issue near internal singularities where the robot displays excessive operational impedance. Conversely, Cartesian space adaptation, demonstrated in [4, 13, 28], demands multiple Jacobian inverse computations at each stage, performing poorly near singularities due to the computational intricacies of the Jacobian inverse.

## 1.1 Paper Contributions

To tackle the prevailing limitations of the current VIC methods, we propose a novel control strategy with the following principal contributions:

1. The proposed algorithm enables the adaptation of impedance parameters in Cartesian space without resorting to the use of the Jacobian inverse. The control formulation take into account both joint-space and operational-space errors in the adaptation of operational-space impedance, obviating the need for the Jacobian inverse in the adaptation. This offers a more efficient and effective method, providing an augmented workspace reach, especially in proximity to kinematic singularities where robot performance exhibits notable improvement.
2. To overcome a common drawback of most existing controllers, the proposed approach equally emphasizes the adaptation and de-adaptation of impedance parameters, thus leading to safer operations in uncertain and unstructured environments.

- tured environments and especially in interaction with humans.
3. The proposed method is shown in a theoretically rigorous manner to guarantee stability and convergence, ensuring safe robot interactions.
  4. Lastly, the proposed controller incorporates high-level learning characteristics inspired by human motor learning, with a particular emphasis on savings. The proposed simplified savings strategy is based on recent developments in human motor learning research [29], and enables the proposed VIC to show accelerated re-learning or savings when re-exposed to previously encountered perturbations or fields.

With these contributions at hand, we now turn our attention toward the synthesis of control that incorporates these aforementioned attributes.

## 2 Control Synthesis

### 2.1 Manipulator Dynamics

Consider the dynamics of an  $n$  degree-of-freedom (DOF) manipulator as

$$\mathbf{M}(\theta)\ddot{\theta}(t) + \mathbf{C}(\theta, \dot{\theta})\dot{\theta}(t) + \mathbf{G}(\theta) = \tau(t) + \tau_{\text{env}}(t), \quad (1)$$

where  $\theta(t) \in \mathbb{R}^n$  is the vector of joint angles,  $t$  is time,  $\mathbf{M}(\theta) \in \mathbb{R}^{n \times n}$  is the inertia-matrix,  $\mathbf{C}(\theta, \dot{\theta}) \in \mathbb{R}^{n \times n}$  is the matrix representing terms for Coriolis and centripetal force,  $\mathbf{G}(\theta) \in \mathbb{R}^n$  is the vector of conservative forces (containing terms related to the potential energy),  $\tau \in \mathbb{R}^n$  is the vector of input torque to the manipulator, and  $\tau_{\text{env}} \in \mathbb{R}^n$  represents torques arising from interactions between the environment and the end-effector. In our model addressing external perturbations, we have taken into account both stiffness and damping factors, while purposefully excluding inertia. This approach is intended to maintain consistency with the system's relative degree and to prevent the non-causality in the system. We assume interaction torques are arising from a combination divergent and error-independent force-fields as

$$\tau_{\text{env}}(t) \triangleq \mathbf{J}^\top(\theta)\mathbf{K}_{x,e}\chi_e(t) + \mathbf{J}^\top(\theta)\mathbf{D}_{x,e}\dot{\chi}_e(t) + \mathbf{J}^\top F_{\text{ext}}, \quad (2)$$

where  $\mathbf{J}(\theta) \in \mathbb{R}^{3 \times n}$  is the manipulator Jacobian,  $\mathbf{K}_{x,e} \in \mathbb{R}^{3 \times 3}$  is the Cartesian-space stiffness of the divergent force-field,  $\chi_e(t) \in \mathbb{R}^3$  is the Cartesian-space position error defined as  $\chi_e(t) \triangleq \chi(t) - \chi_d(t)$ ,  $\chi(t) \in \mathbb{R}^3$  and  $\chi_d(t) \in \mathbb{R}^3$  are end-effector's position and desired position vectors respectively,  $\mathbf{D}_{x,e} \in \mathbb{R}^{3 \times 3}$  is the Cartesian-space damping of the divergent force-field, and  $F_{\text{ext}} \in \mathbb{R}^3$  is external force from

error-independent force-fields. The interaction torque can be expressed in more compact notation as

$$\tau_{\text{env}}(t) \triangleq \mathbf{Z}\mathbf{E}\Phi_x, \quad (3)$$

where,  $\mathbf{Z} \in \mathbb{R}^{n \times 21}$  is the matrix containing Jacobian matrices and defined as

$$\mathbf{Z} \triangleq [\mathbf{J}^\top(\theta), \mathbf{J}^\top(\theta), \mathbf{J}^\top(\theta), \mathbf{J}^\top(\theta), \mathbf{J}^\top(\theta), \mathbf{J}^\top(\theta), \mathbf{J}^\top(\theta)], \quad (4)$$

and  $\mathbf{E} \in \mathbb{R}^{21 \times 21}$  is the block diagonal Cartesian space position error matrix defined as

$$\mathbf{E} \triangleq \text{diag}[\chi_{ex}(t)\mathbf{I}_{3 \times 3}, \chi_{ey}(t)\mathbf{I}_{3 \times 3}, \chi_{ez}(t)\mathbf{I}_{3 \times 3}, \dot{\chi}_{ex}(t)\mathbf{I}_{3 \times 3}, \dot{\chi}_{ey}(t)\mathbf{I}_{3 \times 3}, \dot{\chi}_{ez}(t)\mathbf{I}_{3 \times 3}], \quad (5)$$

where  $\chi_{ex}(t)$ ,  $\chi_{ey}(t)$  and  $\chi_{ez}(t)$  are errors in X, Y, and Z directions of Cartesian-space.  $\mathbf{I}_{3 \times 3}$  is a Identity matrix with  $\mathbf{I}_{3 \times 3} \in \mathbb{R}^{3 \times 3}$ . In Eq. 3,  $\Phi_x \in \mathbb{R}^{21}$  is the vector containing parameters of the external force-field represented as

$$\Phi_x \triangleq \begin{bmatrix} \text{vec}(\mathbf{K}_{x,e}) \\ \text{vec}(\mathbf{D}_{x,e}) \\ F_{\text{ext}} \end{bmatrix}, \quad (6)$$

where  $\text{vec}(\cdot)$  is the column vectorization operator.

### 2.2 Jacobian Aware Adaptive Impedance Control

We now consider a controller for tracking desired trajectories in presence of the external force-field Eq. 3. We define the tracking error vector as

$$\mathcal{S}_\theta(t) \triangleq \dot{\theta}_e(t) + \Lambda\theta_e(t), \quad (7)$$

where  $\theta_e(t) \in \mathbb{R}^n$  is the angular position error defined as  $\theta_e(t) \triangleq \theta(t) - \theta_d(t)$ ,  $\theta_d(t) \in \mathbb{R}^n$  is desired angular position, and  $\Lambda \in \mathbb{R}^{n \times n}$  is a positive definite matrix. The impedance adaptation error is defined as

$$\tilde{\Phi}_x \triangleq \hat{\Phi}_x(t) - \Phi_x, \quad (8)$$

where  $\hat{\Phi}_x(t) \in \mathbb{R}^{21}$  is the adapted Cartesian space impedance. Next, we consider a positive definite candidate Lyapunov function

$$V \triangleq \frac{1}{2}\mathcal{S}_\theta^\top(t)\mathbf{M}(\theta)\mathcal{S}_\theta(t) + \frac{1}{2}\tilde{\Phi}_x^\top(t)\mathbf{P}\tilde{\Phi}_x(t), \quad (9)$$

where  $\mathbf{P} \in \mathbb{R}^{21 \times 21}$  is a positive-definite matrix (note that  $\mathbf{M}(\theta)$  is also positive definite). If  $\dot{V}$  is continuous and

negative-semi-definitive, then stability of the system is guaranteed. Therefore we find a  $\dot{V}$  and strive to derive a control law that yields  $\dot{V}$  continuous and  $\dot{V} \leq 0$ . From Eqs. 7 & 9,

$$\begin{aligned}\dot{V} &= \mathcal{S}_\theta^\top(t)\mathbf{M}(\theta)\dot{\mathcal{S}}_\theta(t) + \tilde{\Phi}_x^\top(t)\mathbf{P}\dot{\tilde{\Phi}}_x(t) \\ &= \mathcal{S}_\theta^\top(t)(\mathbf{M}(\theta)\ddot{\theta}(t) - \mathbf{M}(\theta)\ddot{\theta}_r(t)) + \tilde{\Phi}_x^\top(t)\mathbf{P}\dot{\tilde{\Phi}}_x(t),\end{aligned}\quad (10)$$

where

$$\ddot{\theta}_r(t) = \ddot{\theta}_d(t) - \Lambda\dot{\theta}_e(t).\quad (11)$$

Substituting Eq. 1 in Eq. 10, we get

$$\begin{aligned}\dot{V} &= \mathcal{S}_\theta^\top(t)(\tau(t) + \mathbf{Z}\mathbf{E}\Phi_x - \mathbf{C}(\theta, \dot{\theta})\dot{\theta}(t) - G(\theta) \\ &\quad - \mathbf{M}(\theta)\ddot{\theta}_r(t)) + \tilde{\Phi}_x^\top(t)\mathbf{P}\dot{\tilde{\Phi}}_x(t).\end{aligned}\quad (12)$$

We now consider the control law

$$\tau(t) = \mathbf{M}(\theta)\ddot{\theta}_r(t) + \mathbf{C}(\theta, \dot{\theta})\dot{\theta}(t) + G(\theta) - \mathbf{Z}\mathbf{E}\hat{\Phi}_x(t) - \Lambda\mathcal{S}_\theta(t),\quad (13)$$

where  $\hat{\Phi}_x(t)$  is the adapted impedance. Substituting Eq. 13 in Eq. 12, we get

$$\dot{V} = \mathcal{S}_\theta^\top(t)(-\mathbf{Z}\mathbf{E}\tilde{\Phi}_x(t) - \Lambda\mathcal{S}_\theta(t)) + \tilde{\Phi}_x^\top(t)\mathbf{P}\dot{\tilde{\Phi}}_x(t).\quad (14)$$

The quasi-static nature of the environment field  $\Phi_x$  is assumed, considering the implementation of safety measures to regulate end-effector velocity in the prevalent use of collaborative robots. For instance, the KUKA Sunrise.OS is equipped with a permanent safety measure (PSM) in safety configuration, which halts robot operation when the end-effector velocity surpasses a predetermined threshold. To maintain safety, the reference trajectories for these robots are designed with lower cartesian velocities, thereby ensuring that the impedance parameters at the end-effector varies slowly and their contribution to variations remains insignificant. Therefore, we can consider  $\Phi_x$  to be quasi-static, which implies that  $\dot{\tilde{\Phi}}_x(t) \approx \dot{\hat{\Phi}}_x(t)$ .

From Eq. 14, we then have

$$\dot{V} = -\mathcal{S}_\theta^\top(t)\mathbf{Z}\mathbf{E}\tilde{\Phi}_x(t) - \mathcal{S}_\theta^\top(t)\Lambda\mathcal{S}_\theta(t) + \tilde{\Phi}_x^\top(t)\mathbf{P}\dot{\tilde{\Phi}}_x(t).\quad (15)$$

Further, choosing the adaption law for the impedance as

$$\dot{\tilde{\Phi}}_x(t) = \mathbf{P}^{-1}\mathbf{E}^\top\mathbf{Z}^\top\mathcal{S}_\theta(t),\quad (16)$$

and substituting Eq. 16 in Eq. 15 we get

$$\dot{V} = -\mathcal{S}_\theta^\top(t)\Lambda\mathcal{S}_\theta(t).\quad (17)$$

From Eq. 17 we observe  $\dot{V}$  is continuous and negative-semi-definite, therefore using Barbalat's lemma we conclude  $\lim_{t \rightarrow \infty} \dot{V} = 0$  which leads to  $\lim_{t \rightarrow \infty} \mathcal{S}_\theta = 0$  (since  $\Lambda$  is positive definite) and therefore control law with impedance adaptation law guarantees the convergence of error and asymptotic stability [30]. It is worthwhile to note that the controller adapts the impedance parameter in Cartesian-space without manipulator Jacobian inverse and force sensors. As previously discussed, the control law Eq. 13 and impedance adaptation law Eq. 16 can be utilized independently for Cartesian impedance adaptation. However, the derived controller accumulates impedance over time, failing to de-adapt in the absence of external force fields or low-magnitude force fields. The resulting buildup of impedance presents a risk to human-robot interaction and necessitates costly control efforts. Therefore, we redirect our focus to the synthesis of a technique for the efficient de-adaption of impedance through the use of a variable retention rate (VRR). The retention rate, which is derived from the difference between the estimated and adapted impedance parameters, facilitates effective modulation of the impedance adaptation process and also provides separation between adaptation of error-dependent and dependent force fields.

### 2.3 Force-field Aware Adaptation of Impedance

Using Euler's method of discretization, we represent adaptation law Eq. 16 as

$$\hat{\Phi}_x(t + \Delta t) \approx \hat{\Phi}_x(t) + \Delta t \mathbf{P}^{-1}\mathbf{E}^\top\mathbf{Z}^\top\mathcal{S}_\theta(t).\quad (18)$$

We further reshape Eq. 18 as

$$\hat{\Phi}_x(t + \Delta t) = \Gamma(t)\hat{\Phi}_x(t) + \Delta t \mathbf{P}^{-1}\mathbf{E}^\top\mathbf{Z}^\top\mathcal{S}_\theta,\quad (19)$$

where  $\Gamma(t) \in \mathbb{R}^{21 \times 21}$  is the retention rate (we will discuss a simpler structure for  $\Gamma(t)$  shortly). It is worth noting that if the spectral radius  $\rho(\Gamma) \geq 1$ , then it leads to build up of impedance and if  $\rho(\Gamma) < 1$ , it leads to reduction (or de-adaptation) of impedance. We desire impedance adaptation whenever the controller impedance lags behind the required impedance to provide stable operation in a divergent field, and impedance de-adaptation whenever the controller adapts to a larger impedance than required. Therefore we devise an algorithm for selective modulation of retention rate based on the estimated external force-field. We estimate the external force-field using a disturbance observer [31] and recursive least squares with a forgetting factor [32]. Estimating external disturbance is not feasible with Eq. 1 as it forms an algebraic loop for disturbance estimation; therefore, we utilize the conservation of angular momentum-based disturbance observer, which avoids the measurement/computation of  $\ddot{\theta}(t)$ .

### 2.3.1 Conservation-of-Angular-Momentum-Based Disturbance Observer

The angular momentum  $p(t) \in \mathbb{R}^{n \times 1}$  of the manipulator is  $p(t) = \mathbf{M}(\theta)\dot{\theta}(t)$ .

Using Eq. 1, it then follows that

$$\dot{p}(t) = \dot{\mathbf{M}}(\theta)\dot{\theta}(t) + \tau(t) - \mathbf{C}(\theta, \dot{\theta})\dot{\theta}(t) - G(\theta) + \tau_{\text{env}}(t). \quad (20)$$

The relation between  $\mathbf{M}(\theta)$  and  $\mathbf{C}(\theta, \dot{\theta})$  can be expressed as

$$\dot{\mathbf{M}}(\theta) = \mathbf{C}(\theta, \dot{\theta}) + \mathbf{C}^T(\theta, \dot{\theta}), \quad (21)$$

and substituting Eq. 21 in Eq. 20 yields

$$\dot{p}(t) = \mathbf{C}^T(\theta, \dot{\theta})\dot{\theta}(t) + \tau(t) - G(\theta) + \tau_{\text{env}}(t). \quad (22)$$

However, we don't know  $\tau_{\text{env}}(t)$  and therefore estimate the angular momentum as

$$\dot{\bar{p}}(t) = \mathbf{C}^T(\theta, \dot{\theta})\dot{\theta}(t) + \tau(t) - G(\theta) + k_p(p(t) - \bar{p}(t)), \quad (23)$$

where  $\bar{p}(t)$  is the estimated angular momentum and  $\bar{\tau}_{\text{env}}(t) = k_p(p(t) - \bar{p}(t))$  is used as an estimate of the disturbance torque with  $k_p \in \mathbb{R}^+$  being the proportional gain on estimation error of angular momentum. Next, we estimate external force-field from estimated environmental/disturbance torque and kinematic errors.

### 2.3.2 External Force-Field Estimation using Recursive Least Squares with Forgetting Factor

The relation between the Cartesian-space kinematics-errors and estimated disturbance force is given as

$$\bar{F}_{\text{env}}(t) = [\bar{\mathbf{k}}_{x,e}(t), \bar{\mathbf{d}}_{x,e}(t), \bar{F}_{\text{ext}}(t)] [-\chi_e(t), -\dot{\chi}_e(t), -1]^T, \quad (24)$$

where  $\bar{\mathbf{K}}_{x,e}(t) \in \mathbb{R}^{3 \times 3}$  is the estimated stiffness,  $\bar{\mathbf{D}}_{x,e}(t) \in \mathbb{R}^{3 \times 3}$  is the estimated damping and  $\bar{F}_{\text{env}}(t) \in \mathbb{R}^3$  is estimated the interaction force obtained using estimated disturbance torque and Tikhonov regularisation [33] on manipulator Jacobian as

$$\bar{F}_{\text{env}}(t) = (\mathbf{J}^T \mathbf{J} + \eta \mathbf{I})^{-1} \mathbf{J}^T \bar{\tau}_{\text{env}}(t), \quad (25)$$

with  $\eta \geq 0$  being a parameter for robust inverse near the singularity. It is worthwhile to note that while the adaptation steps were achieved without the need for inverting the Jacobian, Eq. 25 utilizes the Jacobian inverse, however, the

need for this equation can be eliminated through the integration of a force-torque sensor. Further analysis on how it is different from existing approaches is highlighted in the Discussion section. We now estimate the external force-field using recursive least squares as

$$\begin{aligned} \bar{\mathbf{A}}(t + \Delta t) &= \bar{\mathbf{A}}(t) + \frac{\mathbf{L}(t)U(t)}{\lambda + U^T(t)\mathbf{L}(t)U(t)} (\bar{F}_{\text{env}}^T(t) - U^T(t)\bar{\mathbf{A}}(t)), \\ \mathbf{L}(t + \Delta t) &= \left( \mathbf{L}(t) - \frac{\mathbf{L}(t)U(t)U^T(t)\mathbf{L}(t)}{(\lambda + U^T(t)\mathbf{L}(t)U(t)))} \right) \frac{1}{\lambda}, \end{aligned} \quad (26)$$

where  $\bar{\mathbf{A}}(t) = [\bar{\mathbf{K}}_{x,e}(t), \bar{\mathbf{D}}_{x,e}(t), \bar{F}_{\text{ext}}(t)]^T$  and  $\bar{\mathbf{A}} \in \mathbb{R}^{7 \times 3}$ ,  $\bar{U} \in \mathbb{R}^7$  with  $\bar{U}(t) = [-\chi_e(t), -\dot{\chi}_e(t), -1]^T$ ,  $\mathbf{L}(t) \in \mathbb{R}^{7 \times 7}$  being the estimation gain matrix and  $\lambda \in \mathbb{R}$  being the forgetting factor. Next, we compare adapted impedance and estimated impedance for appropriate adaptation and de-adaptation.

### 2.3.3 Modulation of Retention Rate

We modulate the retention rate based on the difference between the norm of estimated impedance (from (26)) and adapted impedance (from (19)) as

$$d_k(t) = (1 + s_f) \|\bar{\mathbf{K}}_{x,e}(t)\|_2 - \|\hat{\mathbf{K}}_{x,e}(t)\|_2, \quad (27)$$

$$d_d(t) = (1 + s_f) \|\bar{\mathbf{D}}_{x,e}(t)\|_2 - \|\hat{\mathbf{D}}_{x,e}(t)\|_2, \quad (28)$$

$$d_f(t) = (1 + s_f) \|\bar{F}_{\text{ext}}(t)\|_2 - \|\hat{F}_{\text{ext}}(t)\|_2, \quad (29)$$

where  $s_f \in \mathbb{R}$  is a safety margin and lower bounded as  $s_f \geq 0$ . Then, a simple and intuitive form for the VRR is

$$\Gamma(t) = \text{diag}[\text{sw}(d_k(t))\mathbf{I}_{9 \times 9}, \text{sw}(d_d(t))\mathbf{I}_{9 \times 9}, \text{sw}(d_f(t))\mathbf{I}_{3 \times 3}], \quad (30)$$

where  $\text{sw}(\cdot)$  is a smooth switching function that returns 1 when difference is positive and return value less than 1 when the difference is negative. A candidate switching function is

$$\text{sw}(d) = \frac{\tanh(ad) + b}{b + 1}, \quad (31)$$

where  $a \in \mathbb{R}$  is the sensitivity gain and  $b \in \mathbb{R}$  is positive scalar. Modulation of retention rate provides appropriate adaption of impedance & force fields for stabilization and reduction in the over-adapted impedance & force when high impedance is not needed. We still require a mechanism for savings as discussed next.

## 2.4 Savings

Recent studies suggest that humans might use an explicit recall strategy for faster re-learning [29]. We capitalize on this observation and devise a mechanism which provides savings.

We consider a situation in which a task is either periodic or a single task is repeatedly performed (multiple trials). For savings, the controller adapts the impedance and force during a trial and forwards the end of the learned impedance and force to the start of the subsequent trial, in other words the last value of the learned impedance and force becomes initial condition for controller in subsequent trial as

$$\hat{\mathbf{K}}_{\text{start,next}} = \hat{\mathbf{K}}_{\text{end,previous}} + \alpha_k \|\theta_e\|_{\text{previous}} \hat{\mathbf{K}}_{\text{end,max}}, \quad (32)$$

$$\hat{\mathbf{D}}_{\text{start,next}} = \hat{\mathbf{D}}_{\text{end,previous}} + \alpha_d \|\theta_e\|_{\text{previous}} \hat{\mathbf{D}}_{\text{end,max}}, \quad (33)$$

$$\hat{\mathbf{F}}_{\text{start,next}} = \hat{\mathbf{F}}_{\text{end,previous}} + \alpha_f \|\theta_e\|_{\text{previous}} \hat{\mathbf{F}}_{\text{end,max}}, \quad (34)$$

where  $\alpha_k, \alpha_d, \& \alpha_f \in \mathbb{R}$  are the proportional gain to the  $\|\cdot\|_{\text{end,max}}$  and  $(\cdot)_{\text{end,max}}$  is the maximum value (at the end of the trial) of the parameter experienced by the controller in the past. This modulation of initial conditions results in savings. Drawing a parallel with human-motor-learning behavior, when errors exceed certain thresholds, people tend to explicitly recall the best course of action from prior experiences in order to maximize performance. It is important to note that this savings strategy is best suited to a situation with force-field aware modulation of adapted impedance as it reduces excessive adapted impedance.

A schematic showing various elements of the proposed controller is presented in Fig. 1.

### 3 Simulation Study: Planar Two Link Serial Chain Manipulator

We now apply the synthesized controller equations to a common robotic system - a planar two-link serial chain manipulator. The dynamics of the robot is expressed in standard manipulator form Eq. 1 with  $M \in \mathbb{R}^{2 \times 2}$ ,  $C \in \mathbb{R}^{2 \times 2}$  and  $G = 0$  (assuming horizontal plane operations).  $\theta \in \mathbb{R}^2$  consists of the two joint angles and  $\tau \in \mathbb{R}^2$  consists of the two joint torques applied to the system. We consider unit lengths of 1 m and unit mass of 1 Kg for both links of the manipulator. The system is fully actuated and the disturbance acting on the system is chosen to be an unstable force-field

disturbance acting on the end-effector given as Eq. 2. The structure of the divergent force-field used for simulations is

$$\mathbf{K}_{x,e} = \mathcal{K} \begin{bmatrix} \cos(\beta) & 0 \\ \sin(\beta) & 0 \end{bmatrix}, \mathbf{D}_{x,e} = \mathcal{D} \begin{bmatrix} \cos(\beta) & 0 \\ \sin(\beta) & 0 \end{bmatrix}, \quad (35)$$

where  $\mathcal{K}$  and  $\mathcal{D}$  are the magnitude and  $\beta$  is the angle for the divergent force-field.

#### 3.1 Simulation Paradigm

We adopt a paradigm similar to one commonly used in human-motor-learning experiments [34]. Each task is a point-to-point reaching task, with a minimum jerk trajectory specified as the desired trajectory. This task is repeated several times, with each instance referred to as a trial, to study the adaptation and de-adaptation behavior of the control algorithm over repetitions of this reaching task. As per the usual practice in human-motor-learning literature, we initially perform several trials - in our case, 50 trials - with no force fields present, referred to as baseline trials. This is followed by a series of 50 trials at a time, during which various aspects of the force field are activated, either one field at a time or in combination, referred to as perturbation trials. These fields are then deactivated for a subsequent 50 trials to observe the de-adaptation behavior, known as washout trials. Finally, the force fields are once again activated for 50 trials at a time to examine the behavior in re-learning or re-adaptation, referred to as re-perturbation trials. Now, we will discuss the results of the simulation.

#### 3.2 Impedance Adaption in Various Directions

We simulate the reaching task with start point (0,0,1) m and stop point (0,1,9) m in x-y plane in 2.5 seconds with  $\mathcal{K} = 450 \frac{\text{N}}{\text{m}}$ ,  $\mathcal{D} = 30 \frac{\text{Ns}}{\text{m}}$ , and constant force-field  $F_{\text{ext}} = [50, 0]^T \text{N}$  with  $\beta = -45, 0, 45$  degrees. We also apply a small random disturbance to trigger the instability. The adaptation gain  $P^{-1} = \text{diag}[6I_{4 \times 4}, 0.3I_{4 \times 4}, 7.5I_{4 \times 4}]$ . Sensitivity gain  $a = 1E5$ , safety margin  $s_f = 0.2$ , and  $b = 500$  are used

**Fig. 1** Block-diagram of proposed controller where numbers represent equation number

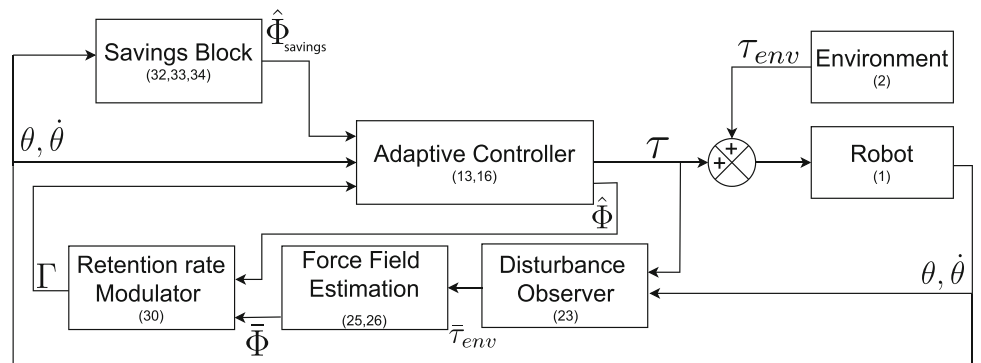




**Fig. 2** Simulated a planar serial-chain manipulator executing a reaching task using our proposed configuration-aware adaptive controller, following the paradigm discussed in Sec. 3.1 and comparable to the experiments in [3]. With all force field components active (only divergent stiffness field is depicted for simplicity), the task was conducted across baseline, perturbation, washout, and re-perturbation trials.

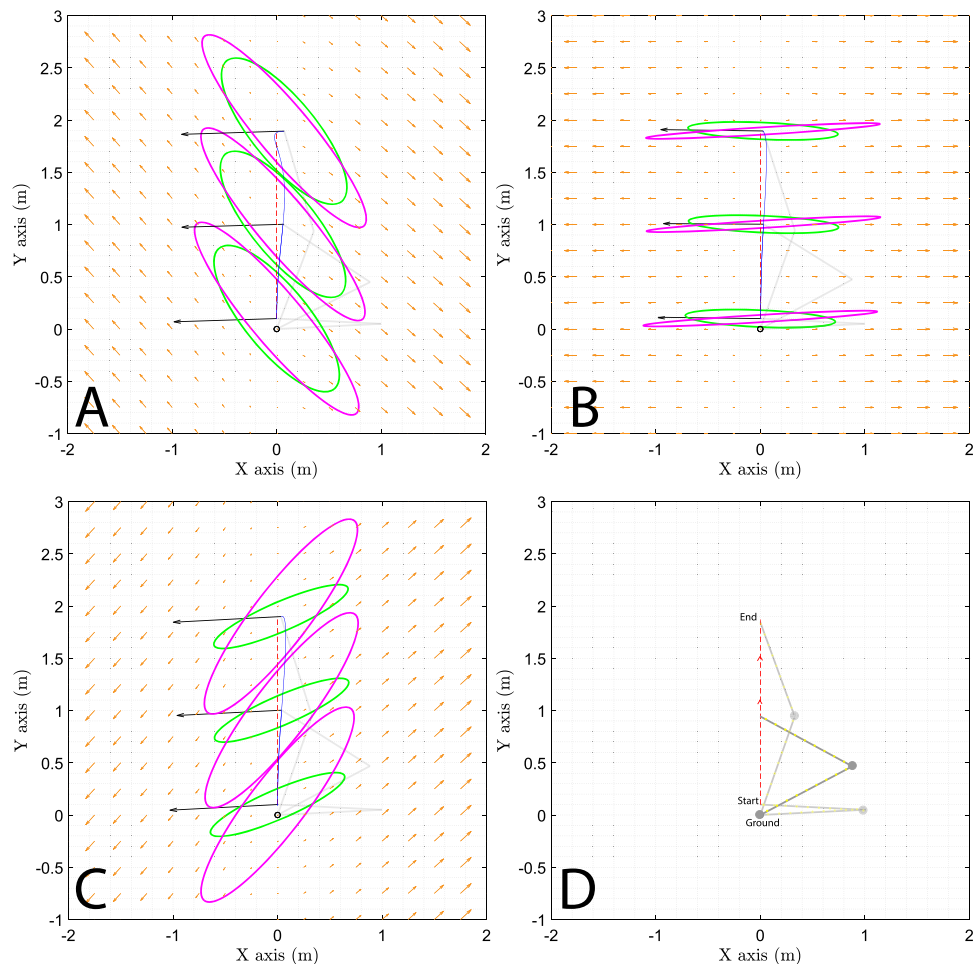
Parameters for trials 50–100 were  $\beta = -45$ ,  $\mathcal{K} = 450$ , and for trials 150–200 were  $\beta = 0$ ,  $\mathcal{K} = 450$ , and  $\beta = 45$ ,  $\mathcal{K} = 450$  respectively. Each curve point denotes the integral of the error for the respective trial. Notably, the controller adapts impedance directionally, stabilizes within a 0.2 safety margin, and smoothly de-adapts post-perturbation

for VRR. For savings we used  $\alpha_k = 0.0035$ ,  $\alpha_d = 0.008$ , and  $\alpha_f = 0.01$  when  $\|\theta_e\| \geq 20$ , and otherwise zero. We used  $K_p = 1E3$ ,  $\lambda = 0.999$ ,  $\eta = 0.01$  near the singularity, and  $\Lambda = I_{2 \times 2}$ . In our proposed method, the controller parameter optimization primarily depends on the control designer who considers various factors. For example, the safety margin relates directly to the noise levels in force sensing, suggesting the need for a higher safety margin under noisy conditions, and vice versa. Sensitivity gains  $a$  and  $b$  adjust the de-adaptation rate, while  $P^{-1}$  directs the adaptation rates, effectively managing the speed

of the controller's impedance adaptation. The selection of savings parameters depends on detected error values, allowing for fine-tuning of the controller's response. This flexible parameter setup enables optimal performance under diverse conditions (Fig. 2).

We represent adapted impedance as the ellipse and adapted force as an arrow, as shown in Fig. 3. The major axis of the adapted impedance ellipse and the arrows representing adapted force, are aligned with the direction of the applied perturbation. Important to note that the area and direction of the ellipse and length of the adapted force remain the

**Fig. 3** Representation of the adapted impedance at the end of each set of perturbation trials shown in Fig. 2. The orange arrows represent the direction and magnitude of the external divergent force-field, the red dashed line represents the reference trajectory for tracking, the actual blue line represents output trajectory, the magenta ellipse represents adapted stiffness, and the green ellipse represents adapted damping, and the black arrow represents adapted force. For plotting, the adapted parameters are divided by the norm of the parameters of applied perturbation (thus a magnitude of 1 represents perfect adaptation). The impedance ellipse and force vector locations are at the traced trajectory's start, middle and end points. In Figures (A), (B), and (C), the robot links are depicted as faint gray lines, while in figure (D), they are represented as gray lines at different configurations



same at the different configurations of the manipulator, which highlights the controller's capability to learn configuration-aware impedance and force. From Figs. 2 & 4, we observe that the adapted impedance and force reaches steady state within the safety margin and de-adapts in the absence of perturbation (Fig. 5).

### 3.3 Independent Estimation and Adaptation of Components of the Force Field with Savings

As mentioned earlier, one challenge in most existing VIC algorithms is that stiffness and damping also adapts even in the presence of error-independent force fields (as highlighted in simulations (phase 1) of [5]). To demonstrate the performance of the proposed controller in such scenarios, we provided perturbations in different phases. After 50 trials of baseline, we provided only the constant force-field for 50 trials, followed by only the divergent stiffness field for the next 50 trials, followed by only the divergent damping field in the next 50 trials (numerical values of the fields are the same as described in Section 3.2). The results in Fig. 4 demonstrates the ability of the controller to independently estimate and adapt to the different components of the field. The controller adaptation is also seen to be faster in the re-perturbation phase (trials 250–400) after a period of washout

(trials 200–250). The faster re-learning is also quantified as a reduction in trapezoidal numerical integration defined as  $\Sigma ||\chi_e||$ , summarized in Table 1.

### 3.4 Comparison with Joint and Cartesian Space Controllers

In our study, we conduct a comprehensive evaluation of controller efficacy, specifically analyzing the performance of the Joint Space Controller (JSC) (similar to [5]) and the Cartesian Space Controller (CSC) (similar to [4]) alongside our proposed controller. The JSC adapts stiffness based on errors in joint position and velocity, concurrently performing dynamics cancellation within the joint space as

$$\tau(t) = \mathbf{M}(\theta)(\ddot{\theta}_d(t) - \mathbf{K}_j(t)(\theta(t) - \theta_d(t)) - \mathbf{D}_j(t)(\dot{\theta}(t) - \dot{\theta}_d(t))) + \mathbf{C}(\theta, \dot{\theta})\dot{\theta}(t) + G(\theta), \quad (36)$$

where  $\mathbf{K}_j \in \mathbb{R}^{n \times n}$  and  $\mathbf{D}_j \in \mathbb{R}^{n \times n}$  are joint space stiffness and damping. And adaptation laws are given as

$$\dot{\mathbf{K}}_j(t) = \gamma_j(t)\mathbf{I}_{n \times n}\text{diag}(\theta_d(t) - \theta(t)) \quad (37)$$

$$\dot{\mathbf{D}}_j(t) = \gamma_j(t)\mathbf{I}_{n \times n}\text{diag}(\dot{\theta}_d(t) - \dot{\theta}(t)). \quad (38)$$

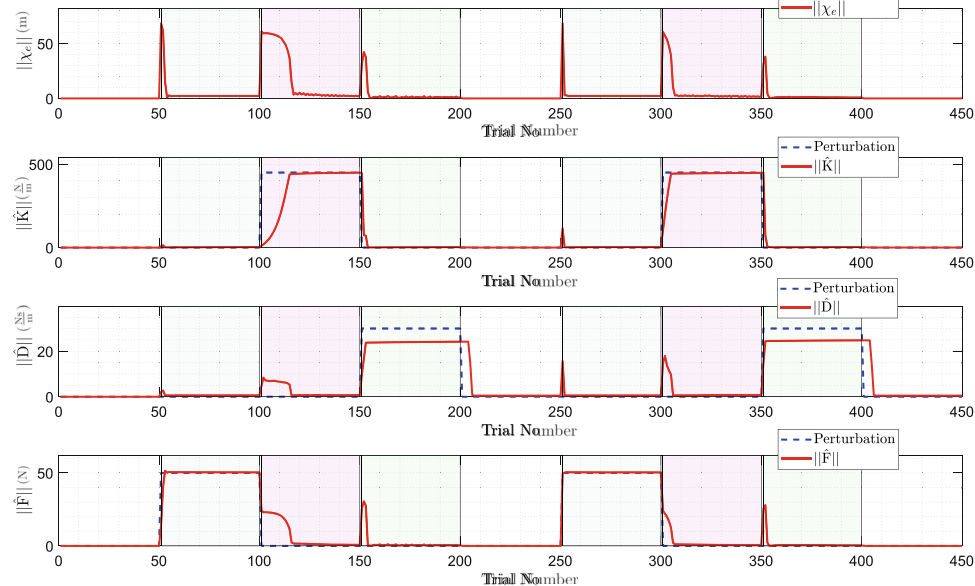


**Fig. 4** Simulation of a planar serial chain manipulator using the proposed controller in the presence of divergent error-based force fields and error-independent force fields. Three phases of perturbation are applied independently of each other; first, the force perturbation, highlighted by the cyan color-second, next, the stiffness perturbation, highlighted by the magenta color-third, and finally, the damping perturbation, high-

lighted by green color. The red line indicates the norm of the parameter evolved over trials, and the dashed blue line represents the norm of the parameters of applied perturbation. The results show that the controller is able to selectively identify and adapt different components of the force field in different sections of the trials

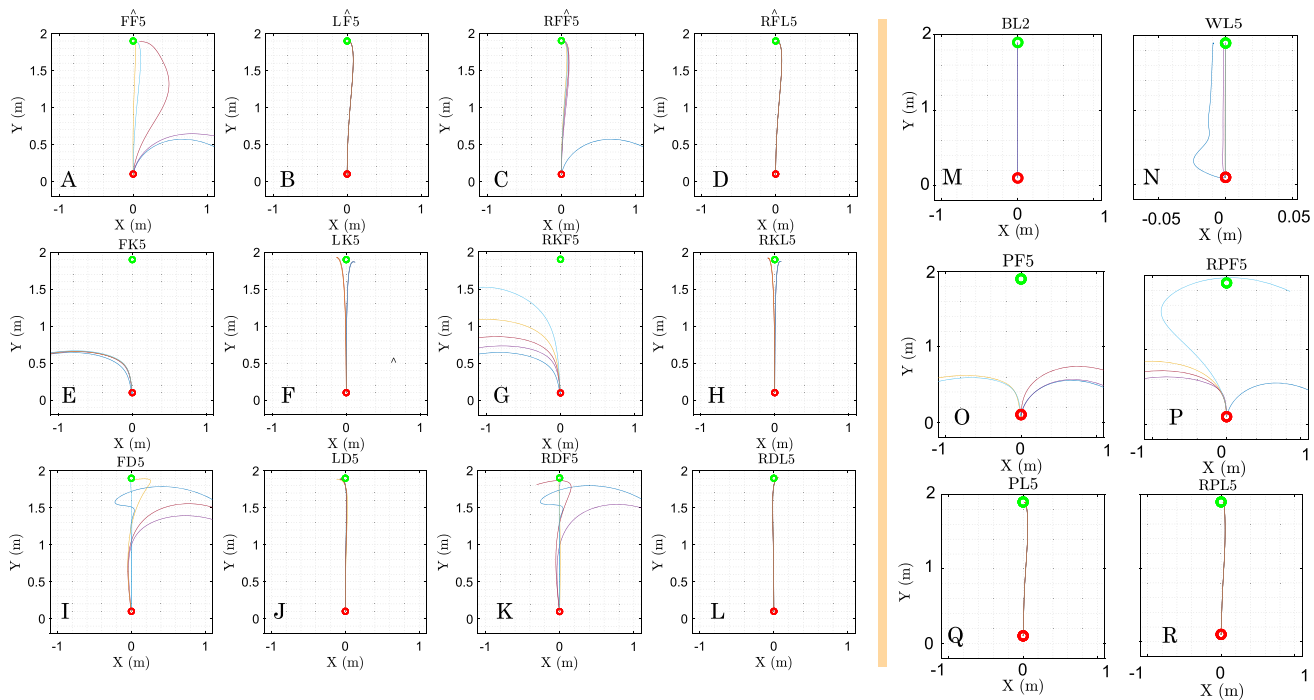


**Fig. 5** Task-space analysis of different adaptation phases shown in Fig. 4 exhibiting faster relearning. Subfigures A to L represents the first and last five trials of different phases of simulation shown in Figure 3. Subfigures M to R represents trials with simultaneous perturbation of  $K = 450 \frac{N}{m}$ ,  $D = 30 \frac{Ns}{m}$ , and  $F_{ext} = [50, 0]^T N$ . The red dot represents a starting point, and the green dot represents the ending point of the

trajectory. In the titles of subfigures, F stands for the first, L stands for the last, the number indicates the number of trials in the plot, B indicates baseline and W represent washout where external perturbations are absent, P indicates perturbation and R indicates re-perturbation. It is observed that in all re-perturbation phases, the controller adopts/learns faster

The  $\gamma_j(t)$  is retention rate and given as

$$\gamma_j(t) = \frac{a_j}{1 + b_j \|\mathcal{S}_\theta(t)\|}, \quad (39)$$

here,  $a_j$  and  $b_j$  are positive constants. On the other hand, the CSC adapts the impedance within the Cartesian space due to errors in Cartesian position and velocity. The control law is given as

$$\begin{aligned} F(t) = & \mathbf{J}^\top \mathbf{M}(\theta) \mathbf{J}^\dagger (\ddot{\chi}_d(t) - \mathbf{K}_x(\chi - \chi_d) - \mathbf{D}_x(\dot{\chi} - \dot{\chi}_d)) \\ & + (\mathbf{J}^\top \mathbf{C}(\theta, \dot{\theta}) \mathbf{J}^\dagger - \mathbf{J}^\top \mathbf{M}(\theta) \mathbf{J}^\dagger \mathbf{J} \mathbf{J}^\dagger) \dot{\chi}(t) + \mathbf{J}^\top G(\theta), \end{aligned} \quad (40)$$

**Table 1** The cost savings associated with various perturbations are assessed through a performance metric defined as the trapezoidal numerical integration of Cartesian space error ( $\Sigma \|\chi_e\|$ )

and the Cartesian space adaptation laws are given as

$$\dot{\mathbf{K}}_x(t) = \gamma_x(t) \mathbf{I}_{n \times n} \text{diag}(\chi_d(t) - \chi(t)) \quad (41)$$

$$\dot{\mathbf{D}}_x(t) = \gamma_x(t) \mathbf{I}_{n \times n} \text{diag}(\mathbf{R}_d(t) - \mathbf{R}(t)). \quad (42)$$

The  $\gamma_x(t)$  is retention rate and given as

$$\gamma_x(t) = \frac{a_c}{1 + b_c \|\mathcal{S}_\chi(t)\|}, \quad (43)$$

here,  $a_c$  and  $b_c$  are positive constants and  $\mathcal{S}_\chi(t)$  is tracking error in Cartesian space. In both controllers the retention rate is based on the tracking error. While this approach is straightforward and computationally efficient, it results in

Type	Perturbation $\Sigma \ \chi_e\ $	Re-perturbation $\Sigma \ \chi_e\ $	Savings
K	215.678	116.914	45.7900%
D	46.587	39.689	14.8100%
F	94.315	70.054	25.7200%
KDF	240.349	125.065	47.9653 %

a slower impedance adaptation in the presence of a large tracking error. Furthermore, if  $a_j < 1$  and the tracking error is zero, the impedance de-adapts in the absence of a force field, setting a constraint on the value of  $a_j$ . When the tracking error converges to zero, the controller begins the impedance de-adaptation process. However, the retention rate defined in equation Eq. 39 can trigger unnecessary de-adaptation, such as when the controller has already adapted the optimal impedance. Consequently, the impedance parameter can fall below the required value, causing the tracking error to become non-zero again, leading to oscillation around zero. The choice of  $a_j$  and  $b_j$  is often empirically determined, and equation Eq. 39 does not differentiate between error-dependent and error-independent impedance parameters. This shortcoming is evident in simulations presented in [5]. These limitations highlight the need for an improved VRR.

In the simulations conducted, each controller is subjected to identical perturbations, ensuring a fair basis for comparison. Figure 6 provides a graphical depiction of the comparative performance attributes of the controllers under study. Subfigure 6A clearly shows the configuration unawareness of the JSC, evidenced by the fluctuating adapted stiffness ellipsoid with the configuration. The value peaks near the singularity, resulting in a higher adaptation than required (since the stiffness matrix is normalized relative to the perturbation magnitude, the ideal range for the major axis should be between -1 and 1, and the minor axis should be minimal, considering the absence of orthogonal perturbations to the field).

Contrary to the JSC, the CSC demonstrates a superior performance, as depicted in Subfigure 6B. It is configuration-aware, and the major axis of the stiffness ellipse remains close

to the -1 to 1 range. However, the substantial minor axis of the ellipse indicates significant impedance adaptation in the minor axis. Unfortunately, this controller's performance degrades near singularity due to multiple Jacobian inversions. The proposed controller (Subfigure C) outperforms the other two controllers, as the adapted stiffness ellipse's major axis falls within the -1 to 1 range, with considerably less adaptation in the orthogonal direction. This controller also maintains efficacy near singularity. It's noteworthy that, due to excessively high adapted stiffness, the JSC exhibits the smallest tracking error, which may not be ideal as it is achieved at the risk of higher impedance in an unstructured and uncertain environment. It is also worth noting that beyond the superiority in performance highlighted in Fig. 6, the proposed controller also incorporates additional features such as de-adaption and savings.

## 4 Experimental Study: KUKA LBR iiwa

We experimentally validate the proposed controller on the KUKA LBR iiwa 7 R800 robot. The experimental methodology adopted in this paper aligns with that outlined in [35]. During the experiments, the robot is subjected to two distinct types of perturbations. The first is a constant weight (480 grams), while the second is a stiffness load ( $67.5 \frac{N}{m}$ ) in the form of a spring assembly attached to the robot's end effector with the other end fixed to a rigid ground. The proposed VIC is implemented for the robot's vertical Cartesian degree of freedom (z), while the horizontal degrees of freedom (x and y) are maintained constant stiffness of  $300 \frac{N}{m}$ . However, applying the proposed controller to the horizontal

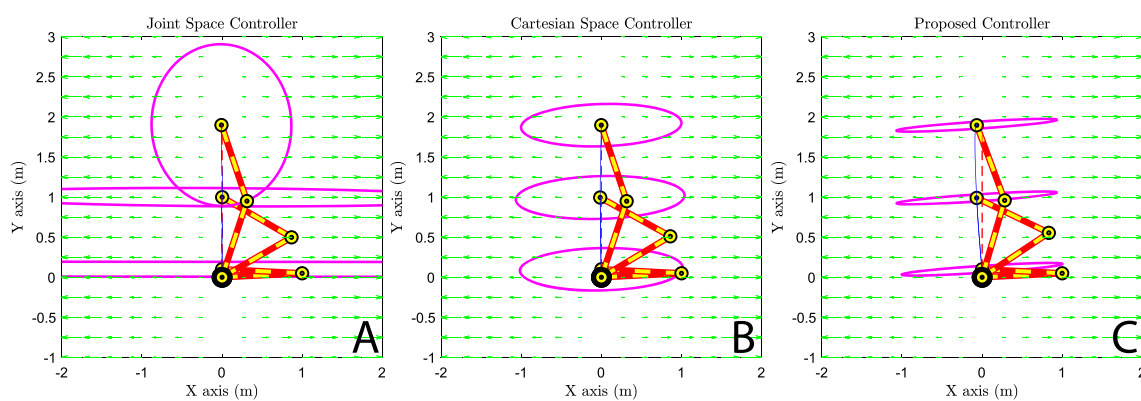


**Fig. 6** Comparative Analysis of Controller Performance: This figure illustrates the comparative attributes of the Joint Space Controller, Cartesian Space Controller, and the proposed controller. Subfigure A highlights the configuration unawareness of the Joint Space Controller, as demonstrated by the fluctuation of the adapted stiffness ellipsoid. Subfigure B showcases the superior, configuration-aware performance

of the Cartesian Space Controllers, however, it has higher impedance adaption in the orthogonal direction of the perturbation. The superior performance of the proposed controller in Subfigure C is underscored by the adapted stiffness ellipse's ideal major axis range and significantly reduced orthogonal adaptation, along with effective operation near the singularity, unlike the Cartesian space controller

Cartesian degrees of freedom can be achieved with straightforward implementation. For the purpose of implementation, the KUKA Sunrise.OS was employed.

#### 4.1 Experimental Paradigm

We perform experiments similar to our simulation paradigm, inspired by human motor learning experiments. Each task entails a point-to-point reaching task with a pre-defined desired trajectory, which is repeated several times (referred to as trials) to investigate the adaptation and de-adaptation behavior of the proposed control algorithm during repeated execution of the reaching task. In line with common practices in human motor literature, we first conduct baseline trials with no externally applied perturbation. We then perform a series of perturbation trials, where constant weight or stiffness disturbances are applied individually. Following the perturbation phase and preceding the re-perturbation phase, wherein identical disturbances are reapplied to assess re-learning or re-adaptation behavior, the adapted impedance and force are reset to zero.

#### 4.2 Force Adaptation

In the experiment aimed at examining the adaptation of force, a reaching task was executed with the starting point

designated in the Cartesian (X,Y,Z) coordinate system as (587,150,230) mm and the terminal point as (587,150,502) mm, taking 3.8 seconds to complete. During the task, a constant external force of magnitude 4.7 N was applied to the end-effector. The data was collected at a sampling rate of 1 kHz. For simplicity, we have adapted the impedance parameters at the start of each trial. The adaptation gain was set to  $P^{-1} = 1.8$ . Additionally, a sensitivity gain of  $a = 10$ , a safety margin of  $s_f = 0.01$ , and a retention rate determined by  $b = 500$  were employed in the experiment. To demonstrate savings, the parameter  $\alpha_f = 0.02$  was utilized when the magnitude of error in the z direction was greater than or equal to 70 mm, otherwise, it was set to zero.

Through the baseline phase, the controller acquires the requisite force information, culminating in minimal tracking error at its termination. During the initial trials of the perturbation and re-perturbation phases, the presence of an additional mass at the end effector of the robot led to a deviation from the desired trajectory and impaired the robot's ability to follow the desired path. The trajectories obtained by employing the proposed trial-by-trial adaptive control, which include the adapted force and corresponding counter-force necessary to counteract the external force, are depicted in Fig. 7. Further, the re-perturbation phase is depicted as a color-matched trial in the figure and it can be seen that the position trajectories converge faster (in few trials) during this phase. The reference trajectories were obtained as the

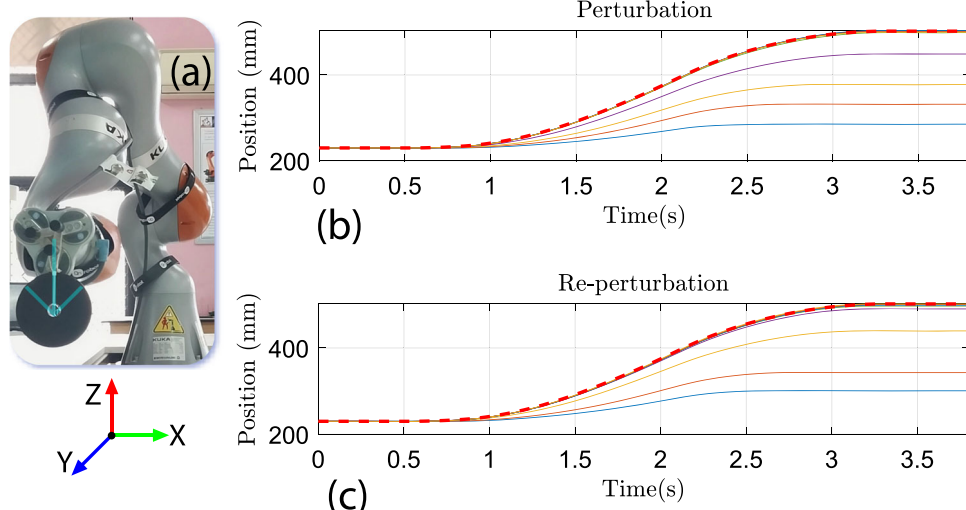


**Fig. 7** Experimental results obtained for the reaching task with the KUKA LBR iiwa R800 using the proposed controller in the presence of a constant external force perturbation of 4.7 N at the end-effector. The robot adapts the necessary force to counteract the external weight in a trial-by-trial manner, and upon re-introduction of the same perturbation after resetting earlier force estimates to zero, the robot demonstrates a faster re-learning process. Subfigure (a) illustrates the robot is executing the reaching task while counteracting the gravitational force in the

Z-direction, as highlighted by cyan arrow. Subfigures (b) and (c) depict the end-effector's position in the Z-direction during the perturbation and re-perturbation phases, respectively. The red dashed line represents the baseline trajectory when no external force is applied. The trials are color-matched and demonstrated with the first trial indicated by the blue line, the second by orange, and so on. In the re-perturbation phase, the trials are closer to the desired trajectory compared to those in the perturbation phase

average of last baseline trajectories recorded in the absence of external forces. Additionally, the error plot in Fig. 8 also indicates that the adaptation occurs at a faster rate during the re-perturbation phase, as evidenced by the quicker convergence of the error. Additionally, the controller also de-adapts the applied force when it exceeds the required force, enhancing the safety of the interaction, as illustrated in Fig. 8.

### 4.3 Stiffness Adaptation

The experiment aimed at investigating the adaptation of stiffness was conducted using a similar reaching task, where the starting point in the Cartesian coordinate system (X, Y, Z) was designated as (589, 151, 342) mm and the terminal point as (589, 151, 530) mm, with a completion time of 5.35 seconds. A stiffness load was applied to the end-effector during the task, which was composed of two springs (of  $135 \frac{N}{m}$ ) in series configuration, resulting in a load of  $67.5 \frac{N}{m}$ . The data was collected at a sampling rate of 1 kHz and for ease of interpretation, the impedance parameters were adjusted at the start of each trial. The experiment utilized an adaptation gain of  $P^{-1} = 1.8$ , a sensitivity gain of  $a = 10$ , a safety margin of  $s_f = 0.01$ , and a retention rate specified by  $b = 500$ . To demonstrate savings, the parameter  $\alpha_k = 0.02$  was employed when the magnitude of error in the z direction exceeded 70 mm, otherwise it was set to zero.

In the initial trials of the perturbation and re-perturbation phases, the presence of an external stiffness load at the end-

effector resulted in a deviation from the desired trajectory, hindering the robot's ability to follow the intended path. The proposed trial-by-trial adaptive control approach is able to adapt the required stiffness and the corresponding counterforce required to counteract the external stiffness, are presented in Fig. 10.

Moreover, the re-perturbation phase is depicted as a color-coded trial in the Fig. 9 and it is evident that the position trajectories are more closely aligned with the reference trajectories during this phase. The reference trajectories were obtained as the average of last baseline trajectories recorded in the absence of external forces. Similar to the experiment on external force adaptation, the error plot in Fig. 10 also demonstrates a faster rate of adaptation during the re-perturbation phase, as evidenced by the quicker convergence of the error.

## 5 Discussion

We've introduced a configuration and force-field-aware VIC. The proposed controller adapts impedance parameters in Cartesian space without Jacobian inverse reliance, improving efficiency and workspace reach, particularly near kinematic singularities. Balancing impedance parameter adaptation and de-adaptation, the proposed method considers both error-dependent and error-independent environment fields. Parameter estimation and adaptation optimization use a smooth switching law and integrate high-level learning fea-

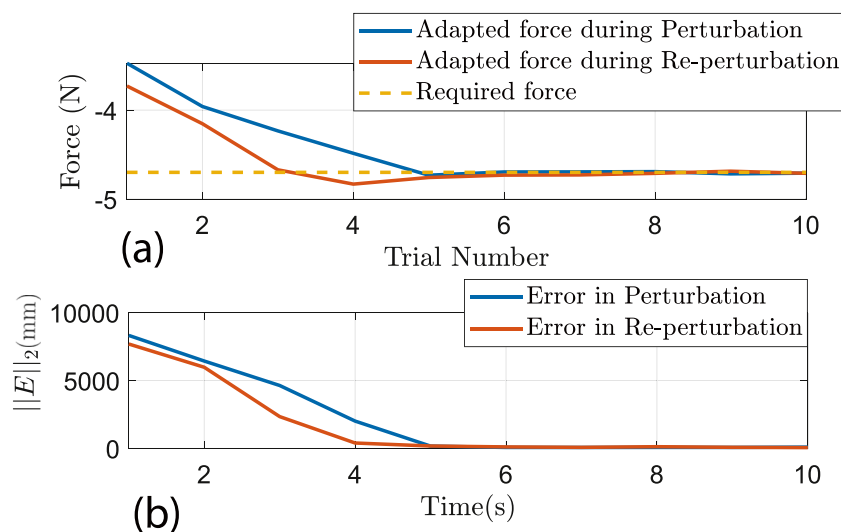


**Fig. 8** Experimental results obtained for the reaching task using the KUKA LBR iiwa R800 robot and the proposed controller, in the presence of an external force perturbation of 4.7 N applied at the end-effector. The evolution of the adapted force and norm of tracking error over each trial, as depicted in subfigure (a), demonstrate that the robot exhibited an adaptive response to the external force, adjusting the force it applied to overcome the perturbation and eventually settling to the

desired force value. It is important to note that the controller de-adapted the force when it overshot the required force. During the re-perturbation phase, the robot demonstrated a faster adaptation of the applied force compared to the initial perturbation phase. The performance of the robot was evaluated using the norm of the end-effector's position error, and as shown in subfigure (b), faster convergence of the error was observed during the re-perturbation phase

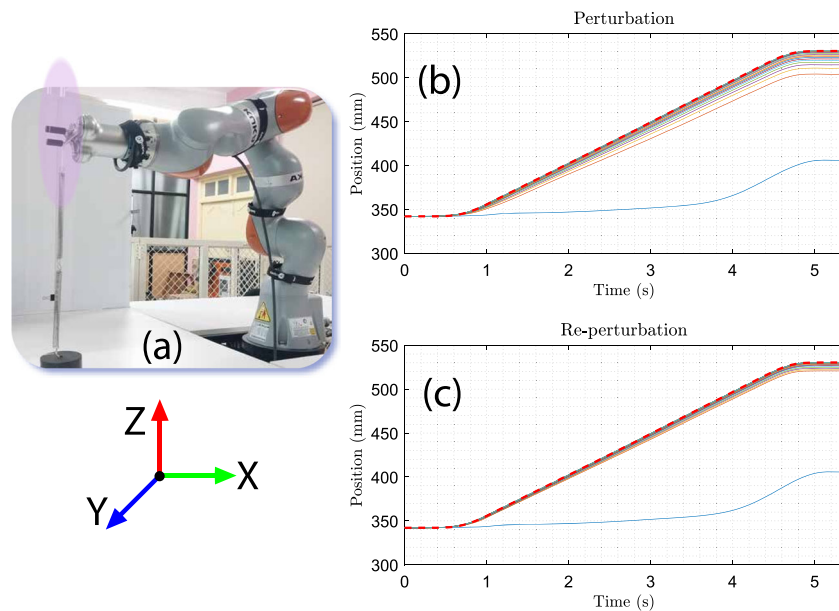


**Fig. 9** Experiments were conducted using the KUKA LBR iiwa R800 and the proposed controller, to examine the performance of the robot under an external stiffness perturbation of  $67.5 \frac{N}{m}$  at the end-effector during a reaching task. The results demonstrate that the robot adapts its stiffness in a trial-by-trial manner to counteract the external stiffness load, and shows a faster re-learning when the same perturbation is reintroduced. Subfigure (a) displays the robot executing the reaching task while compensating for the stiffness load in the Z-direction,

highlighted by magenta ellipsoid. Subfigures (b) and (c) present the end-effector's position in the Z-direction during the perturbation and re-perturbation phases, respectively. In the absence of external force, the baseline trajectory is depicted by the red dashed line. The color-coded trials are displayed, with the blue line representing the first trial, the orange line representing the second trial, and so on. During the re-perturbation phase, the trials exhibit greater proximity to the desired trajectory when compared to the trials during the perturbation phase

tures from human motor learning for rapid re-adaptation. The proposed controller's effectiveness was experimentally validated on a 7-DOF KUKA iiwa robot using a simple reaching task.

The adaptation of impedance in robotic manipulators can be achieved in either the joint space or the operational Car-

tesian space of the robot. Traditional VICs concentrate on the adaptation of impedance in the joint space. However, the relationship between Cartesian space impedance parameters and joint space impedance parameters is established through the robot's Jacobian, which is a function of the robot's configuration. Consequently, the same Cartesian space impedance

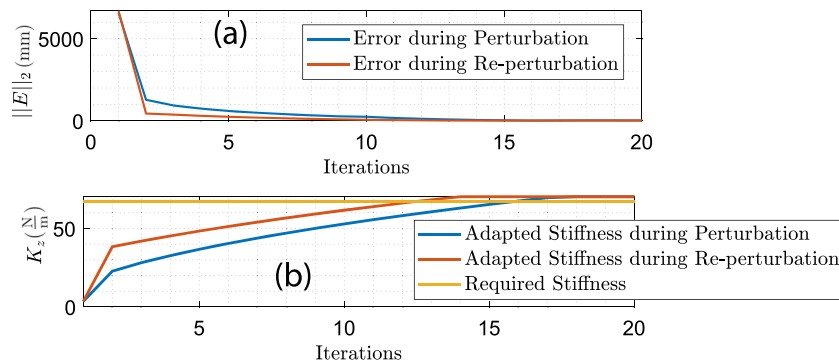


**Fig. 10** Experiments were conducted to evaluate the performance of the proposed controller in the presence of an external stiffness load of  $67.5 \frac{N}{m}$  applied at the end-effector of the KUKA LBR iiwa R800 robot. The results, as depicted in subfigure (a), indicate that the robot was able to adapt its applied stiffness in response to the external perturbation, ultimately settling to the desired stiffness values. During the

re-perturbation phase, the robot showed an improved adaptation of the applied stiffness compared to the initial perturbation phase. The performance of the robot was assessed using the norm of the end-effector's position error and, as depicted in subfigure (b), a faster convergence of the error was observed during the re-perturbation phase

results in different joint space impedances at different configurations given as

$$\mathbf{K}_j = \mathbf{J}(\theta)^T \mathbf{K}_x \mathbf{J}(\theta) + \frac{\partial \mathbf{J}(\theta)^T}{\partial \theta} F_{ext}, \quad (44)$$

where  $\mathbf{K}_j \in \mathbb{R}^{n \times n}$  is a joint space stiffness,  $\mathbf{J}(\theta) \in \mathbb{R}^{3 \times n}$  is a manipulator Jacobian,  $\mathbf{K}_x \in \mathbb{R}^{3 \times 3}$  is a Cartesian space stiffness, and  $F_{ext}$  is the external force. The task trajectory leads to various robot configurations, some of which may result in either higher or lower impedance values in the joint space for the same Cartesian space impedance. In such scenarios, adaptive controllers typically adjust the impedance values towards higher ones to maintain stability constraints, leading to higher impedance adaptation than necessary at certain robot configurations, as depicted in Fig. 6A.

To circumvent the problem of configuration-sensitive impedance adaptation, several authors[4, 28, 36–39] have formulated the robot dynamics in the Cartesian space as

$$\mathbf{J}^T \dot{\mathbf{M}}(\theta) \mathbf{J}^T \ddot{x}(t) + (\mathbf{J}^T \dot{\mathbf{C}}(\theta, \dot{\theta}) \mathbf{J}^T - \mathbf{J}^T \dot{\mathbf{M}}(\theta) \mathbf{J}^T \dot{\mathbf{J}} \mathbf{J}^T) \dot{x}(t) + \mathbf{J}^T G(\theta) = F(t). \quad (45)$$

However, this approach necessitates the computation of multiple Jacobian inverses, potentially reducing the effective workspace due to the challenges of inverting the Jacobian near kinematic singularities. The controller proposed in this method adapts the Cartesian space impedance as described in Eqs. 46, 47 without the need for multiple Jacobian inverses as in Eq. 45. Nevertheless, the proposed controller assumes that the external impedance parameters vary slowly, imposing velocity constraints suitable for tasks with collaborative robots operating within these constraints. The control law and the adaption law for the controller are

$$\tau(t) = \mathbf{M}(\theta) \ddot{\theta}_r(t) + \mathbf{C}(\theta, \dot{\theta}) \dot{\theta}(t) + G(\theta) - \mathbf{Z} \mathbf{E} \hat{\Phi}_x(t) - \Lambda \mathcal{S}_\theta(t), \quad (46)$$

and

$$\dot{\hat{\Phi}}_x(t) = \mathbf{P}^{-1} \mathbf{E}^T \mathbf{Z}^T \mathcal{S}_\theta(t). \quad (47)$$

The adaptive controller Eqs. 46, 47 with error based retention rate Eq. 43 operates without using the Jacobian inverse. However, like prior adaptive impedance controllers, it's prone to over-adaptation of impedance under noisy feedback conditions and tends to maintain an unnecessarily high adapted impedance after external force fields are eliminated. These issues underscore the need for a VRR alongside the adaptive impedance controller. Our proposed VRR, given by Eq. 30, outperforms prior methods by more effectively managing the adaptation and de-adaptation of impedance parameters. It also allows for selective adaptation of error-dependent and error-independent impedance parameters. This method relies on comparing estimated

impedance parameters with adapted ones. However, this step requires the use of the Jacobian inverse and is computationally intensive. This step requiring inversion of the Jacobian can be eliminated when employing a force-torque sensor. Future work will concentrate on reducing the complexity of this method to devise a solution that is less resource-intensive while preserving its advantages. Future experiments will focus on dynamic conditions, including grinding and polishing operations, as well as force production tasks that involve instabilities, such as using an extended screwdriver for fastening applications. Additionally, the algorithm's applicability in human-robot collaborative tasks may be investigated, particularly its capacity for real-time impedance adjustment to facilitate coordination with human operators.

Finally, the proposed controller incorporates human-motor-learning features such as savings and retention, which find practical applications in robotic systems. While their significance is clear, these features were absent in earlier VIC methods. The proposed approach for embedding savings in VIC echoes the human approach of referencing past successful actions. However, it's essential to combine this with the new VRR to manage potential impedance increases, ensuring timely de-adaptation when needed. Overall, the presented controller approach provides an efficient way to incorporate savings in VIC, ushering in notable advancements in robotics.

## 6 Conclusion

In this study, we have designed a novel variable impedance controller that incorporates several distinctive features. These features include the prevention of over-adaptation of impedance, independent estimation and adaptation to distinct components of environmental force fields, configuration-aware adaptation to circumvent issues resulting from the inversion of Jacobian, and the provision of stabilization guarantees through a Lyapunov-function-based approach. To demonstrate the effectiveness of our proposed controller, we conducted simulations using a serial-chain manipulator that was subjected to various combinations of divergent force fields, and experiments using a seven-degree-of-freedom KUKA iiwa robot. Our results show that the proposed algorithm is capable of faster relearning when exposed to force fields encountered in the past. However, the limitations of our framework include the requirement for knowledge of the manipulator's parameters, which is similar to previous variable impedance control based on Lyapunov or passivity theory. Furthermore, our controller is better suited to tasks that involve lower end-effector velocities as it assumes that the external force field varies slowly.

**Acknowledgements** The authors wish to gratefully acknowledge appreciation to Prof. Asokan Thondiyath and lab members of the V M Thomas Robotics Research and Teaching Laboratory, at the Indian Institute of Technology Madras, for generously hosting S. Jadav at IIT Madras and permitting full access to the KUKA robot in their lab. We extend our sincere gratitude for the time and effort invested by the reviewers, which have been instrumental in enhancing the quality of the manuscript.

#### Author Contributions

1. Research project:
    - (a) Conception
    - (b) Organization
    - (c) Execution
  2. Experiments & Analysis:
    - (a) Design
    - (b) Execution
    - (c) Review and Critique
  3. Manuscript Preparation:
    - (a) Writing of the first draft
    - (b) Review and Critique
- SJ: 1a, 1b, 1c, 2a, 2b, 3a.  
HPM: 1a, 1b, 2a, 2c, 3b.

**Funding** This research endeavor is funded through two grants from the Science and Engineering Research Board (SERB): the Core Research Grant (CRG/2022/005196) and the MATRICS Grant (MTR/2021/000225).

**Availability of data and material** The datasets used during the current study are available from the corresponding author upon reasonable request.

#### Declaration

**Competing interests** The authors declare that they have no conflict of interest.

**Consent for publication** Both authors provided consent for publication.

#### References

1. Mussa-Ivaldi, F.A., Hogan, N., Bizzi, E.: Neural, mechanical, and geometric factors subserving arm posture in humans. *J. Neurosci.* **5**(10), 2732–2743 (1985). <https://doi.org/10.1523/jneurosci.05-10-02732.1985>
2. Burdet, E., Osu, R., Franklin, D.W., Milner, T.E., Kawato, M.: The central nervous system stabilizes unstable dynamics by learning optimal impedance. *Nature* **414**(6862), 446–449 (2001). <https://doi.org/10.1038/35106566>
3. Franklin, D.W., Liaw, G., Milner, T.E., Osu, R., Burdet, E., Kawato, M.: Endpoint stiffness of the arm is directionally tuned to instability in the environment. *J. Neurosci.* **27**(29), 7705–7716 (2007). <https://doi.org/10.1523/jneurosci.0968-07.2007>
4. Li, Y., Ganesh, G., Jarrassé, N., Haddadin, S., Albu-Schaeffer, A., Burdet, E.: Force, impedance, and trajectory learning for contact tooling and haptic identification. *IEEE Trans. Robot.* **34**(5), 1170–1182 (2018). <https://doi.org/10.1109/tro.2018.2830405>
5. Yang, C., Ganesh, G., Haddadin, S., Parusel, S., Albu-Schaeffer, A., Burdet, E.: Human-like adaptation of force and impedance in stable and unstable interactions. *IEEE Trans. Robot.* **27**(5), 918–930 (2011). <https://doi.org/10.1109/tro.2011.2158251>
6. Krakauer, J.W., Hadjiosif, A.M., Xu, J., Wong, A.L., Haith, A.M.: Motor learning. *Compr Physiol* **9**(2), 613–663 (2019). <https://doi.org/10.1002/cphy.c170043>
7. Mathew, J., Lefévre, P., Crevecoeur, F.: Savings in human force field learning supported by feedback adaptation. *Eneuro* **8**(5) (2021). <https://doi.org/10.1523/eneuro.0088-21.2021>
8. Kami, A., Meyer, G., Jezzard, P., Adams, M.M., Turner, R., Ungerleider, L.G.: Functional mri evidence for adult motor cortex plasticity during motor skill learning. *Nature* **377**, 155–158 (1995). <https://doi.org/10.1038/377155a0>
9. Halsband, U., Lange, R.K.: Motor learning in man: a review of functional and clinical studies. *Journal of Physiology-Paris* **99**(4–6), 414–424 (2006). <https://doi.org/10.1016/j.jphysparis.2006.03.007>
10. Abu-Dakka, F.J., Saveriano, M.: Variable impedance control and learning—a review. *Front. Robot. AI* **7** (2020). <https://doi.org/10.3389/frobt.2020.590681>
11. Brohan, A., Brown, N., Carbajal, J., Chebotar, Y., Dabis, J., Finn, C., Gopalakrishnan, K., Hausman, K., Herzog, A., Hsu, J., Ibarz, J., Ichter, B., Irpan, A., Jackson, T., Jesmonth, S., Joshi, N., Julian, R., Kalashnikov, D., Kuang, Y., Leal, I., Lee, K.-H., Levine, S., Lu, Y., Malla, U., Manjunath, D., Mordatch, I., Nachum, O., Parada, C., Peralta, J., Perez, E., Pertsch, K., Quiambao, J., Rao, K., Ryoo, M.S., Salazar, G., Sanketi, P.R., Sayed, K., Singh, J., Sontakke, S., Stone, A., Tan, C., Tran, H., Vanhoucke, V., Vega, S., Vuong, Q.H., Xia, F., Xiao, T., Xu, P., Xu, S., Yu, T., Zitkovich, B.: RT-1: Robotics Transformer for Real-World Control at Scale. In: Proceedings of Robotics: Science and Systems, Daegu, Republic of Korea (2023). <https://doi.org/10.15607/RSS.2023.XIX.025>
12. Yang, C., Jiang, Y., He, W., Na, J., Li, Z., Xu, B.: Adaptive parameter estimation and control design for robot manipulators with finite-time convergence. *IEEE Trans. Ind. Electron.* **65**(10), 8112–8123 (2018). <https://doi.org/10.1109/tie.2018.2803773>
13. Ferraguti, F., Preda, N., Manurung, A., Bonfe, M., Lambery, O., Gassert, R., Muradore, R., Fiorini, P., Secchi, C.: An energy tank-based interactive control architecture for autonomous and teleoperated robotic surgery. *IEEE Trans Robot* **31**(5), 1073–1088 (2015). <https://doi.org/10.1109/tro.2015.2455791>
14. Michel, Y., Ott, C., Lee, D.: Safety-aware hierarchical passivity-based variable compliance control for redundant manipulators. *IEEE Trans Robot* **38**(6), 3899–3916 (2022). <https://doi.org/10.1109/tro.2022.3174478>
15. Sun, T., Peng, L., Cheng, L., Hou, Z.-G., Pan, Y.: Stability-guaranteed variable impedance control of robots based on approximate dynamic inversion. *IEEE Trans. Syst. Man Cybern. Syst* **51**(7), 4193–4200 (2019). <https://doi.org/10.1109/tsmc.2019.2930582>
16. Kronander, K., Billard, A.: Stability considerations for variable impedance control. *IEEE Trans. Robot.* **32**(5), 1298–1305 (2016). <https://doi.org/10.1109/tro.2016.2593492>
17. Zhuang, Z., Tao, H., Chen, Y., Stojanovic, V., Paszke, W.: An optimal iterative learning control approach for linear systems with nonuniform trial lengths under input constraints. *IEEE Trans. Syst. Man Cybern. Syst* **53**(6), 3461–3473 (2023). <https://doi.org/10.1109/TSMC.2022.3225381>
18. Zhou, C., Tao, H., Chen, Y., Stojanovic, V., Paszke, W.: Robust point-to-point iterative learning control for constrained systems: A minimum energy approach. *Int. J. Robust Nonlinear Control* **32**(18), 10139–10161 (2022) <https://onlinelibrary.wiley.com/doi/pdf/10.1002/rnc.6354> <https://doi.org/10.1002/rnc.6354>
19. Stulp, F., Buchli, J., Ellmer, A., Mistry, M., Theodorou, E.A., Schaal, S.: Model-free reinforcement learning of impedance control in stochastic environments. *IEEE Trans Auton Ment Dev* **4**(4), 330–341 (2012). <https://doi.org/10.1109/tamd.2012.2205924>
20. Roveda, L., Testa, A., Shahid, A.A., Braghin, F., Piga, D.: Q-learningbased model predictive variable impedance control for physical humanrobot collaboration. *Artif Intell* **312**, 103771 (2022). <https://doi.org/10.1016/j.artint.2022.103771>

21. Roveda, L., Maskani, J., Franceschi, P., Abdi, A., Braghin, F., Molinari Tosatti, L., Pedrocchi, N.: Model-based reinforcement learning variable impedance control for human-robot collaboration. *J Intell Robot Syst* **100**(2), 417–433 (2020). <https://doi.org/10.1007/s10846-020-01183-3>
22. Bogdanovic, M., Khadiv, M., Righetti, L.: Learning variable impedance control for contact sensitive tasks. *IEEE Robot. Autom. Lett.* **5**(4), 6129–6136 (2020). <https://doi.org/10.1109/LRA.2020.3011379>
23. Song, X., Sun, P., Song, S., Stojanovic, V.: Quantized neural adaptive finite-time preassigned performance control for interconnected nonlinear systems. *Neural Comput. Appl.* **35**(21), 15429–15446 (2023). <https://doi.org/10.1007/s00521-023-08361-y>
24. Roveda, L., Pallucca, G., Pedrocchi, N., Braghin, F., Tosatti, L.M.: Iterative learning procedure with reinforcement for high-accuracy force tracking in robotized tasks. *IEEE Trans. Ind. Inform.* **14**(4), 1753–1763 (2017). <https://doi.org/10.1109/tii.2017.2748236>
25. Zhang, X., Sun, L., Kuang, Z., Tomizuka, M.: Learning variable impedance control via inverse reinforcement learning for force-related tasks. *IEEE Robot. Autom. Lett.* **6**(2), 2225–2232 (2021). <https://doi.org/10.1109/lra.2021.3061374>
26. Khader, S.A., Yin, H., Falco, P., Krugic, D.: Stability-guaranteed reinforcement learning for contact-rich manipulation. *IEEE Robot. Autom. Lett.* **6**(1), 1–8 (2020). <https://doi.org/10.1109/lra.2020.3028529>
27. Piovesan, D., Pierobon, A., DiZio, P., Lackner, J.R.: Experimental measure of arm stiffness during single reaching movements with a time-frequency analysis. *J. Neurophysiol.* **110**(10), 2484–2496 (2013). <https://doi.org/10.1152/jn.01013.2012>
28. Li, Y., Ge, S.S.: Human-robot collaboration based on motion intention estimation. *IEEE/ASME Trans Mechatron* **19**(3), 1007–1014 (2013). <https://doi.org/10.1109/tmech.2013.2264533>
29. Sadaphal, D.P., Kumar, A., Mutha, P.K.: Sensorimotor learning in response to errors in task performance. *Eneuro* **9**(2) (2022). <https://doi.org/10.1523/eneuro.0371-21.2022>
30. Slotine, J.-J.E., Li, W., et al.: *Appl Nonlinear Control* **199**(1) (1991)
31. Van Damme, M., Beyl, P., Vanderborght, B., Grosu, V., Van Ham, R., Vanderniepen, I., Matthys, A., Lefeber, D.: Estimating robot end-effector force from noisy actuator torque measurements. In: 2011 IEEE international conference on robotics and automation, pp. 1108–1113 (2011). <https://doi.org/10.1109/icra.2011.5980210> IEEE
32. Johnstone, R.M., Johnson, C.R., Jr., Bitmead, R.R., Anderson, B.D.: Exponential convergence of recursive least squares with exponential forgetting factor. *Syst. Control. Lett.* **2**(2), 77–82 (1982). [https://doi.org/10.1016/s0167-6911\(82\)80014-5](https://doi.org/10.1016/s0167-6911(82)80014-5)
33. Golub, G.H., Hansen, P.C., O’Leary, D.P.: Tikhonov regularization and total least squares. *SIAM J. Matrix Anal. Appl.* **21**(1), 185–194 (1999). <https://doi.org/10.1137/s0895479897326432>
34. Shadmehr, R., Wise, S.: Supplementary documents for “Computational Neurobiology of Reaching and Pointing”. Cambridge, MA: MIT Press (2005). <https://doi.org/10.1080/09548980701275714>
35. Li, C., Zhang, Z., Xia, G., Xie, X., Zhu, Q.: Efficient force control learning system for industrial robots based on variable impedance control. *Sensors* **18**(8) (2018). <https://doi.org/10.3390/s18082539>
36. Sharifi, M., Zakerimanesh, A., Mehr, J.K., Torabi, A., Mushahwar, V.K., Tavakoli, M.: Impedance variation and learning strategies in human-robot interaction. *IEEE Trans Cybern* **52**(7), 6462–6475 (2021)
37. Ferraguti, F., Secchi, C., Fantuzzi, C.: A tank-based approach to impedance control with variable stiffness. In: 2013 IEEE international conference on robotics and automation, pp. 4948–4953 (2013). <https://doi.org/10.1109/ICRA.2013.6631284>
38. Enayati, N., Mariani, S., Wahrburg, A., Zanchettin, A.M.: Variable impedance and force control for robust learning of contact-rich manipulation tasks from user demonstration. *IFAC-PapersOnLine* **53**(2), 9834–9840 (2020). <https://doi.org/10.1016/j.ifacol.2020.122687> 21st IFAC World Congress
39. Shahriari, E., Kramberger, A., Gams, A., Ude, A., Haddadin, S.: Adapting to contacts: Energy tanks and task energy for passivity-based dynamic movement primitives. In: 2017 IEEE-RAS 17th international conference on humanoid robotics (Humanoids), pp. 136–142 (2017). IEEE

**Publisher’s Note** Springer Nature remains neutral with regard to jurisdictional claims in published maps and institutional affiliations.

Springer Nature or its licensor (e.g. a society or other partner) holds exclusive rights to this article under a publishing agreement with the author(s) or other rightsholder(s); author self-archiving of the accepted manuscript version of this article is solely governed by the terms of such publishing agreement and applicable law.

**Shail Jadav** currently pursuing a Ph.D. in Mechanical Engineering at the Indian Institute of Technology Gandhinagar (IIT Gandhinagar), focuses on robotics, control theory, and biomedical engineering. He obtained his B.E. in Biomedical Engineering from Gujarat Technological University in 2017. Following his undergraduate studies, he was part of the research staff at IIT Gandhinagar from 2017 to 2018, before embarking on his doctoral studies in 2018.

**Dr. Harish Palanthandlam-Madapusi** is an Associate Professor of Mechanical Engineering at the Indian Institute of Technology Gandhinagar (IIT Gandhinagar), and has interests in robotics, control systems, and their applications. He has worked at IIT Bombay (2001–2002), Syracuse University (2007–2011), and has been at IIT Gandhinagar since 2011. He has also held leadership positions at IIT Gandhinagar and has been its first Associate Dean and subsequently Dean of Campus Development (2015–2018), Dean of Student Affairs at IIT Gandhinagar (2018–2020), and is currently the Dean of General administration. Dr. Harish received the B.E. degree from the University of Mumbai in mechanical engineering in 2001 and the Ph.D. degree from the Aerospace Engineering Department at the University of Michigan in 2007.